AEGC2019 Data to Discovery
Australasian Exploration Geoscience Conference
2-5 September 2019 • Perth, Western Australia
Incorporating the AIG, ASEG, PESA, and WABS

Inverting the head wave coefficient with multi-fold near-surface seismic refraction data

Derecke Palmer
The University of New South Wales
Sydney 2052 Australia
d.palmer@unsw.edu.au

SUMMARY

The head wave coefficient (HWC), the refraction analogue of the reflection coefficient, is a complex function of the densities and the P- and S-wave velocities in both the weathered and sub-weathered regions. In general, the HWC increases with increasing P- and S-wave velocities in the weathered layer, but it decreases with increasing P- and S-wave seismic velocities in the sub-weathered layer.

Unscaled S-wave velocities in the weathered and sub-weathered regions can be computed with the HWCs for each interface and the detailed P-wave seismic velocities in each layer, using various approximations for the HWC. In general, there is excellent agreement between the measured and computed HWCs. However, some form of traveltime-based estimate of the S-wave velocities is required to calibrate the amplitude-based estimates.

Key words: refraction, amplitudes, head wave coefficient, inversion, S-wave velocities

THE WIRRINYA PROFILE

This study inverts the head wave coefficient (HWC), the refraction analogue of the reflection coefficient, for a 2 km section of the Wirrinya traverse 99WR-HR1, which was recorded over 17 km of the Palaeozoic Lachlan Fold Belt in south-eastern Australia. This section has been selected because detailed models of the P-wave velocities in the sub-weathered region have been computed previously from the traveltime data with 1.5D and 2D inversion algorithms (Palmer, 2015). The various refraction tomograms, which exhibit considerable spatial variations in the seismic velocities in the sub-weathered region, are representative of a moderately complex geological environment. Furthermore, it is anticipated that a lateral change in the seismic velocities in the weathered layer, which occurs between stations 1465 and 1500, will have a significant effect on the HWC.

THE P-WAVE APPROXIMATION TO THE HWC

Whereas the derivations of the reflection coefficients were published over a century ago, those for the HWC have proven to be somewhat more challenging (Heelan, 1953; Werth, 1967; Červený and Ravindra, 1971). They involve the P- and S-wave seismic velocities and the densities in both the weathered and sub-weathered regions, and without exception, all are quite complex. The different formulations are discussed in Meulenbroek (2016).

Červený and Ravindra (1971, Figure 3.11), computed the head wave coefficient for a uniform 1D two-layer model, for a range of density ratios ρ_1/ρ_2, and seismic velocity ratios β_1/α_1 and β_2/α_2, where α and β are the P- and S-wave velocities. They concluded that the influence of the density and the velocity ratios in the weathered layer is not large. However, they concluded that the influence of the velocity ratios in the sub-weathered layer to be considerable, with increasing values of β_2/α_2 resulting in increasing values of the head wave coefficient. In fact, for any combination of the ratios β_1/α_1 and β_2/α_2, the head wave coefficient is an increasing function of α_1/α_2.

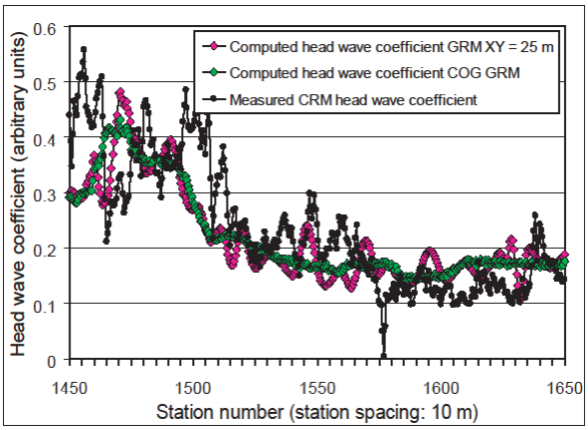

Figure 1: Comparison of measured and computed head wave coefficients using P-wave seismic velocities computed with the traveltimes.

The formal mathematical expressions for K, the HWC, are quite complex (e.g. Palmer, 2001, Equation 2), and simple approximations are generally preferred, as is also the case with the Zoeppritz Equations with reflection methods. The approximation in Equation 1 (Palmer, 2001, Equation 3), constitutes a useful starting point.

$$K \propto 2\,\frac{\rho_1 \propto_1}{\rho_2 \propto_2} \qquad (1)$$

Figure 1 compares the head wave coefficient computed with the P-wave seismic velocities measured in Palmer (2015, Figures 19 and 21) but ignoring any variations in the density ratio, with the measured HWC computed with the multi-fold CRM. The correlation between the measured and computed HWCs is generally quite reasonable. The higher values between stations 1450 and 1525 correspond approximately with the higher seismic velocities in the weathered layer of 1750 m/s between stations 1450 and 1500. The head wave coefficients also correspond with a lower seismic velocity in the sub-weathered layer of ~5000 m/s between stations 1450 and 1525. Also, the lower HWCs correspond with higher seismic velocities of

~6000 m/s between stations 1575 and 1650. Furthermore, the frequent short wavelength coincidences between the various graphs demonstrate that the HWC is responding to the detailed spatial variations in the seismic velocities in the sub-weathered layer.

Nevertheless, the correspondence with the P-wave seismic velocities as validated with refraction tomography is not precise.

S-WAVE VELOCITIES IN THE P-WAVE HWC

The computation of the HWC in Figure 1, suggests that the P-wave seismic velocities in the weathered and sub-weathered layers, alone, are insufficient to fully account for the observed head wave coefficients. Given the considerable spatial variations in the P-wave seismic velocities in both layers, it is reasonable to anticipate that similar variability probably occurs with the S-wave seismic velocities. Furthermore, and consistent with the results of Červený and Ravindra (1971, Figure 3.11), the fundamental physical mechanisms for the generation and propagation of the refracted signal, suggest that the S-wave velocities might be significant.

Seismic energy propagates in a predominantly vertical direction with reflection seismology. The partition of energy at the interface with representative petrophysical properties (Sheriff and Geldart, 1995), demonstrates that there is minimal mode conversion at near-vertical incidence. As a result, the normal incidence Zoeppritz Equations, which employ the P-wave velocities only, are generally quite adequate, because most of the particle motion is compressional. Nevertheless, some account of the S-wave velocities can be necessary with large offsets, as is the case with AVO.

By contrast, seismic energy propagates in a predominantly horizontal direction with refraction seismology. With the traditional P-wave model of the seismic refraction process, the seismic energy propagating along the top of the sub-weathered region represents compressional P-wave energy. However, the transmission of that seismic energy back into the weathered region includes a shear coupling process at the interface. Accordingly, it is reasonable to anticipate that the S-wave velocities might have an important influence on the head wave coefficient.

However, the challenge with the inclusion of the S-wave seismic velocities in any analysis is that the theoretical expressions for the HWC are quite complex, when all seismic velocities and densities are included. For the simplified analysis in this study, as well as for the building of starting models for detailed inversion, convenient approximations are desirable. Equation 2 below is an approximation derived from the Equation of Werth (1967; Palmer, 2001, Equation 2).

$$K \cong 8 \frac{\rho_1 \alpha_1}{\rho_2 \alpha_2 \left(2\left(\rho_1/\rho_2\right)^2 + 1\right)} \left(\frac{\beta_2}{\beta_1}\right)^2 \qquad (2)$$

In the absence of suitable data, it will be assumed that the S-wave velocities essentially parallel the P-wave velocities in the weathered layer, that is, β_1/α_1 can be treated as approximately constant. Also, the density in the sub-weathered region, and the ratio of the density to the P-wave velocity in the weathered layer also will be assumed constant.

Accordingly, Equation 2 can be simplified and rearranged to give:

$$\frac{\beta_2}{\alpha_2} \approx \left(\frac{K \rho_2 \alpha_1}{2 \rho_1 \alpha_2}\right)^{1/2} \frac{\beta_1}{\alpha_1} \qquad (3)$$

Equation 3 can be simplified even further to give:

$$\beta_2 \approx (K \alpha_2)^{1/2} \qquad (4)$$

The results are presented in Figure 2.

In most fresh or slightly weathered igneous and metamorphic rocks, the ratio of S-wave to P-wave seismic velocities exhibits a small range of values, commonly 0.5-0.7 (Cox, 1999). Since the P-wave velocities in the sub-weathered layer range from approximately 5000 m/s to 6000 m/s, it is reasonable to anticipate a range of approximately 3000 m/s to 3500 m/s for the S-wave velocities.

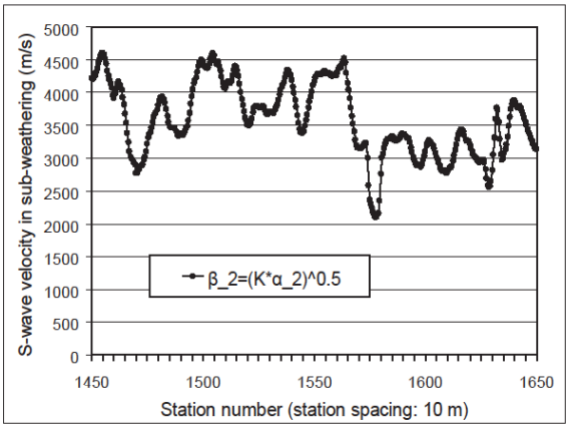

Figure 2: S-wave velocity in the sub-weathered layer derived from the P-wave velocity and the head wave coefficient.

Rather than increasing along the profile in sympathy with the P-wave velocities in the sub-weathered region, the S-wave velocities decrease in sympathy with the head wave coefficient, which in turn, largely decreases with the P-wave velocity in the weathered region. Nevertheless, and irrespective of the uncertainties in the scaling of the HWC and the many approximations in Equation 4, Figure 2 demonstrates that the S-wave velocities between stations 1575 and 1650 are unusually low when compared to those between stations 1450 and 1575.

MODELLING THE HWC WITH THE WERTH EQUATION

Figures 1 and 2, and the various approximations in Equations 1-4, confirm that the HWC is a complex function of the P- and S-wave seismic velocities in both the weathered and sub-weathered regions. An assessment of the usefulness of these approximations can be obtained by evaluating the exact Werth expression for the HWC, using a range of computed and assumed parameters.

So far, it has been assumed that the densities do not vary greatly within either the weathered or sub-weathered regions. Now however, spatial variations in the densities are computed with a representative value for each region (1.8 tonnes/m^3 in the

weathered layer and 2.5 tonnes/m^3 in the sub-weathered layer) which are then multiplied by the scaled P-wave velocities to the one quarter power (Sheriff and Geldart, 1995, Equation 5.15). Although not shown here, the computed head wave coefficients are relatively insensitive to a representative range of density functions, as is also demonstrated by Červený and Ravindra (1971, Figure 3.11).

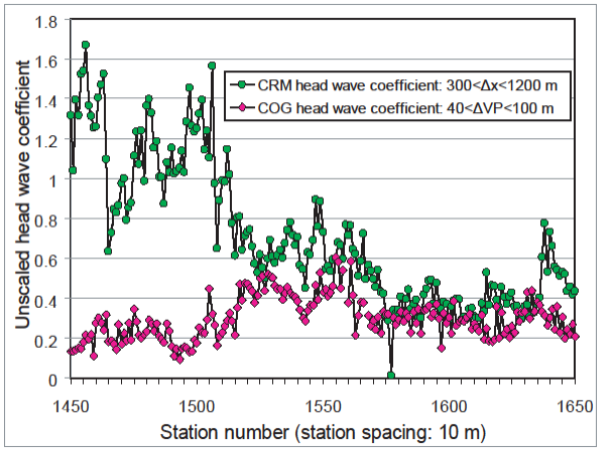

Figure 3: Unscaled head wave coefficients computed with near and far trace offsets.

By contrast, representative values for the S-wave velocities initially proved to be a little more challenging. In theory, it should be possible to obtain good estimates from surface wave inversion. However, in this study, the 10 m receiver interval results in significant spatial aliasing. The final approach was to compute the S-wave velocity in the sub-weathered layer, with the approximation of Equation 2, using the S-wave velocity in the weathered layer, computed with the approximation in Equation 4.

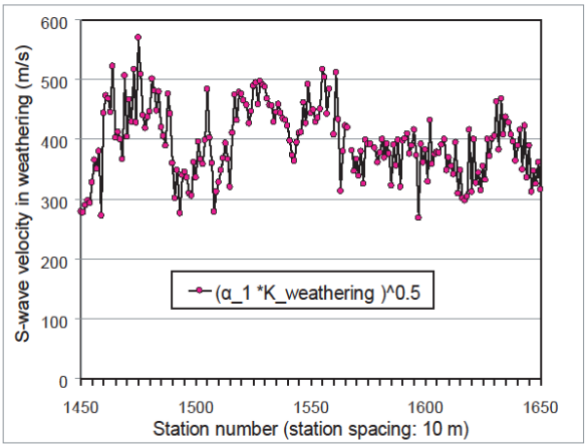

Figure 4: S-wave velocity in the weathered layer computed with the P-wave velocity and the head wave coefficient in the weathered layer.

The HWC for the weathered layer was computed from the head wave amplitudes for the near trace arrivals with the COG GRM, and it is shown in Figure 3. The apparent mirror imaging of the two sets of HWCs is the result of the P-wave velocity in the weathered layer appearing in the numerator with the sub-weathered layer values and in the denominator with the weathering values. The computed S-wave velocity in the weathered layer is shown in Figure 4.

The results are presented in Figures 5-7. In general, the fit between the computed and the measured HWCs is exceptional. In fact, the near-perfect fit might even prompt a spontaneous expression of scientific scepticism! To use a well-known idiom, is the fit "too good to be true?"

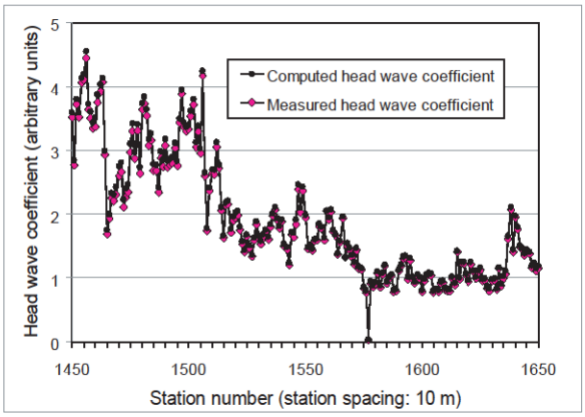

Figure 5: Comparison of measured and computed head wave coefficients.

Notwithstanding, one significant measure of verisimilitude is the observation that these results demonstrate a remarkable consistency between the HWCs computed from different sets of amplitudes with different source-to-receiver offsets from different refractors. It parallels the recursive sequential layer-by-layer approach of the standard traveltime methods, such as the ITM. In fact, it indicates that a similar recursive approach might be appropriate with routine head wave inversion.

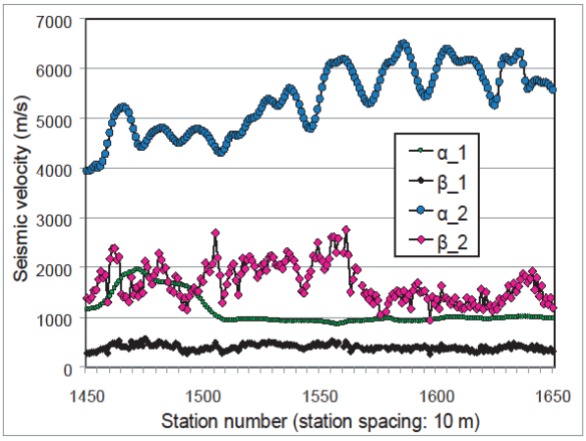

Figure 6: Summary of P- and S-wave seismic velocities which reproduce the observed head wave coefficients in the weathered and sub-weathered regions.

Furthermore, the measured HWCs have not been smoothed, in order to minimise the effects of any variability in the surface soil layers, or receiver coupling. Any variations due to very near surface variations in the soil layers have been automatically accommodated in the HWCs computed with the arrivals from the top of the weathered layer. It demonstrates an alternate method of correcting for any amplitude "statics."

The most important conclusion which can be drawn from these results is that the various assumptions made in Equations 2 and 4 can be reasonable under suitable conditions. The many assumptions made in Equation 4 are applicable in the derivation of the S-wave velocities in the weathered layer, but not necessarily in the sub-weathered layer. Furthermore, the derivation of the S-wave velocities in the sub-weathered layer with Equation 2, is facilitated by the computation of the S-wave velocities in the weathering with Equation 4. Nevertheless, there is always a concern with the reality of non-uniqueness, in addition to the scaling of the S-wave velocities as discussed below.

The fit between the observed and measured HWCs is essentially independent of the scaling required to convert the approximation in Equation 4 into an absolute S-wave velocity in the weathered layer. Although not shown here, a range of scaling factors produces equivalent agreement. It is consistent with the fact that most formulations for the HWC are expressed in terms of dimensionless velocity ratios, rather than absolute seismic velocities. It can be concluded that some form of traveltime-based estimate of the S-wave velocities is required for calibration of the unscaled amplitude-based estimates.

As indicated in Figure 2 with simple approximations of the head wave coefficient in Equation 4, the S-wave velocities in the sub-weathering between stations 1575 and 1650 decrease, whereas the P-wave velocities increase. This feature is emphasised in Figure 7 with the S- to P-wave velocity ratio derived from the values in Figure 6.

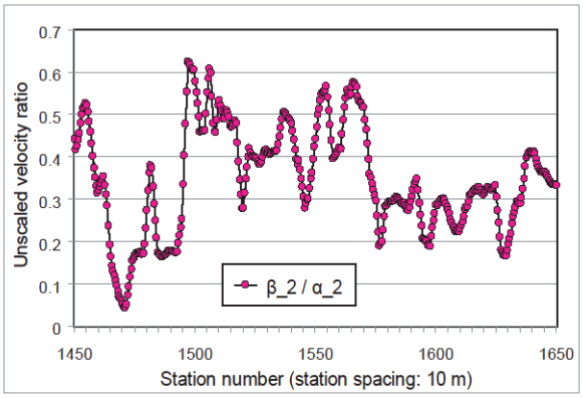

Figure 7: Unscaled ratio of S- to P-wave seismic velocities in the sub-weathered region.

The rocks in this region of the study area are Ordovician turbidites of the Kirribilli Formation, which have been metamorphosed to greenschist facies. The unit is generally tightly to isoclinally folded and fine grained metamorphic muscovite commonly defines a penetrative weak to strong foliation, usually developed only in the finer-grained rocks. The foliation in shales and phyllites becomes strong to intense in the vicinity of major structures.

It can be concluded that the unusually low S-wave velocities represent the occurrence of a pronounced rock fabric, that is, the velocities may be a de facto qualitative measure of seismic anisotropy.

By contrast, the lower S- to P-wave velocity ratio in the vicinity of station 1470 corresponds with a probable thrust fault.

CONCLUSIONS

The head wave coefficient is a complex function of the densities and the P- and S-wave velocities in both the weathered and sub-weathered regions. In general, the HWC increases with increasing P- and S-wave velocities in the weathered layer, but it decreases with increasing P- and S-wave seismic velocities in the sub-weathered layer.

Unscaled S-wave velocities in the weathered and sub-weathered regions can be computed with the HWCs for each interface and the detailed P-wave seismic velocities in each layer, using various approximations for the HWC. In general, there is excellent agreement between the measured and the computed HWCs. However, some form of traveltime-based estimate of the S-wave velocities is required to calibrate the amplitude-based estimates.

It is anticipated that these inverted parameters will be applicable in their own right with current routine geotechnical investigations. Furthermore, quite detailed starting models can also be generated for more computationally intensive approaches, such as full waveform inversion, as these methods systematically become realistic, reliable and routine with near surface refraction data.

REFERENCES

Červený, V., Ravindra, R., 1971, Theory of seismic head waves, Toronto, University of Toronto Press.

Cox, M. J. G., 1999, Static corrections for seismic reflection surveys. Society of Exploration Geophysicists, Tulsa.

Heelan, 1953, On the theory of head waves. *Geophysics*, 18, 871-893.

Meulenbroek, A. M., 2016. Inversion of seismic refraction amplitudes for near-surface velocity control. M Ph thesis, Univ. of Queensland, 313p.

O'Brien, P. N. S., 1967, The use of amplitudes in seismic refraction survey, in Musgrave, A.W., Ed., Seismic refraction prospecting: Society of Exploration Geophysicists, 85–118.

Palmer, D, 2001, Resolving refractor ambiguities with amplitudes, *Geophysics* 66, 1590-1593.

Palmer, D., 2015, Is accuracy more important than precision in near surface refraction seismology? *Near Surface Geophysics*, 13, 1-18.

Sheriff, R. E., and Geldart, L. P., 1995, Exploration seismology: Cambridge Univ. Press.

Werth,G. A., 1967, Method for calculating the amplitude of the refraction arrival, in Musgrave, A.W., Ed., Seismic refraction prospecting: Society of Exploration Geophysicists, 119–137.